Molecular dissection of the actin-binding ability of the fission yeast α-actinin, Ain1, *in vitro* and *in vivo*

Rikuri Morita, Masak Takaine[$], Osamu Numata, and Kentaro Nakano*

Department of Biological Sciences, Graduate School of Life and Environmental Sciences, University of Tsukuba, 1-1-1 Tennohdai, Tsukuba, Ibaraki 305-8572, Japan

[$]Present address: Gunma University Initiative for Advanced Research (GIAR), Gunma University, 3-39-15 Showa-machi, Maebashi, Gunma 371-8512, Japan

Running title: in vitro and in vivo activities of *S. pombe* Ain1

*Correspondence to: Kentaro Nakano, Department of Biological Sciences, Graduate School of Life and Environmental Sciences, University of Tsukuba, 1-1-1 Tennohdai, Tsukuba, Ibaraki 305-8572, Japan

Tel.: +81-29-853-6642

Fax: +81-29-853-6642

E-mail: knaknao@biol.tsukuba.ac.jp

Summary

A contractile ring (CR) is involved in cytokinesis in animal and yeast cells. Although several types of actin-bundling proteins associate with F-actin in the CR, their individual roles in the CR have not yet been elucidated in detail. Ain1 is the sole α-actinin homologue in the fission yeast *Schizosaccharomyces pombe* and specifically localizes to the CR with a high turnover rate. *S. pombe* cells lacking the *ain1*$^{+}$ gene show defects in cytokinesis under stress conditions. We herein investigated the biochemical activity and cellular localization mechanisms of Ain1. Ain1 showed weaker affinity to F-actin *in vitro* than other actin-bundling proteins in *S. pombe*. We identified a mutation that presumably loosened the interaction between two calponin-homology domains constituting the single actin-binding domain (ABD) of Ain1, which strengthened the actin-binding activity of Ain1. This mutant protein induced a deformation in the ring shape of the CR. Neither a truncated protein consisting only of an N-terminal ABD nor a truncated protein lacking a C-terminal region containing an EF-hand motif localized to the CR, whereas the latter was involved in the bundling of F-actin *in vitro*. We herein propose detailed mechanisms for how each part of the molecule is involved in the proper cellular localization and function of Ain1.

Keywords: actin, actin-bundling protein, contractile ring, cytokinesis, fission yeast

Introduction

The contractile ring (CR), which mainly consists of filamentous actin (F-actin) and myosin-II, induces the formation of a cleavage furrow during cytokinesis in animal and yeast cells. Several types of actin-modulating proteins control the properties and behavior of F-actin in the CR (*1*, *2*). The bundling of F-actin may be indispensable for maintaining the microstructure and overall architecture of the CR. However, contraction of the CR, which is mediated by an interaction between F-actin and myosin II, may be suppressed if F-actin is too tightly bundled. This may apply not only to the CR, but also to the large number of actomyosin-sliding systems responsible for cell migration and movement. Moreover, the three-dimensional structure of the actin cytoskeleton and its mechanical properties may be significantly affected by the presence of actin-bundling proteins that directly determine the number of cross-linking sites, the distance and angle between filaments, and plasticity of the cytoskeletal structure. This may explain why various types of actin-bundling proteins are found in eukaryotic cells.

Several members of the calponin superfamily play important roles in the bundling of F-actin. Calponin is strongly expressed in smooth muscle cells and controls actomyosin activity (*3*). Approximately 100 a. a. in the N-terminal half of this protein is called the calponin-homology domain (CHD). Various actin-bundling proteins utilize their CHDs as an interface to interact with F-actin (*4*, *5*). IQGAP is one of the actin-bundling proteins, the function of which has been characterized in detail both *in vivo* and *in vitro* (*6–9*). This protein forms a dimer and bundles F-actin by binding to different F-actins with the N-terminal CHD of each subunit (*10*). A previous study reported that IQGAP and its homologue localized to the CR of various types of cells including the sea urchin fertilized egg (*11*), cultured mammalian cells (*12*, *13*), the budding yeast *Saccharomyces cerevisiae* (*14*), and the fission yeast *Schizosaccharomyces pombe* (*15*). Furthermore, another single CHD-containing protein Stg1, a homologue of the SM22/transgelin-like protein, was found in the division site of an *S. pombe* cell; however, unlike the IQGAP-homologue Rng2, its function was not essential for the progression of cytokinesis (*16*).

On the other hand, many actin-bundling proteins utilize a double repeat of CHDs as a single actin-binding domain (ABD). Filamin forms a dimer and exerts F-actin-bundling activity through the N-terminal ABD of each subunit (*17*). This protein is found in a cleavage furrow in vertebrate cells (*18*, *19*). The cellular slime mold *Dictyostelium discoideum* has homo- and hetero-dimeric actin-bundling proteins, called cortexillin-I, -II, and -III, which are involved in cytokinesis (*20*, *21*). Cortexillin-I bundles F-actin with its C-terminal short tail instead of its N-terminal ABD (*22*). An ABD has also been found in the actin-bundling proteins fimbrin and α-actinin. Fimbrin consists of a tandem repeat of double ABDs in a single molecule, and each ABD binds to different F-actins. Previous studies demonstrated that fimbrin localizes to the CR in the ciliate *Tetrahymena* (*23*) and *S. pombe* cells (*24*, *25*). α-Actinin forms an anti-parallel dimer via its spectrin-like repeats (SRs) located in the middle of the molecule and bundles F-actin. In mammalian cells, α-actinin is involved in controlling the ingression rate of the cleavage furrow (*26*). The α-actinin homologue Ain1 has also been identified in the CR of *S. pombe* cells (*25*).

The molecular mechanisms underlying the formation of the CR have been extensively investigated in the fission yeast *S. pombe*, and the cytokinetic functions of actin-bundling proteins have been studied in detail (*15*, *16*, *23*, *24*, *27*, *28*). Of these, only IQGAP Rng2 and α-actinin Ain1 show CR-limited localization (15, 25), while other actin-bundling proteins such as fimbrin Fim1 and Stg1 are also found in actin patches, a different actin cytoskeleton engaged in endocytosis, in this organism (*16*, *24*, *25*). Rng2 plays an essential role in the proper organization of F-actin in the CR (*15*, *27*). However, mutant cells, in which the chromosomal *rng2*$^{+}$ gene is replaced with the truncated gene encoding N-terminal CHD-lacking Rng2, still remain and undergo cell division (*28*). Therefore, some actin-bundling proteins may redundantly function with Rng2 in cytokinesis in this organism. Functional relationships between Rng2, Ain1, and Fim1 have been detected in *S. pombe* (*24*, *25*). Similar to mammalian α-actinin, Ain1 contains three functional moieties: N-terminal ABD, SRs in the middle region, and the C-terminal EF-hand motif. A previous study demonstrated that cytokinesis failed in *ain1*-null cells exposed to stress conditions and synthetic lethality occurred with the simultaneous gene deletion of *fim1*$^{+}$ (*25*). Moreover, Ain1 appears to cooperatively

promote the formation of the CR with myosin-II Myo2 (*29*). However, the biochemical and structural characterization of Ain1 had not been performed until recently (*30*, *31*). We herein evaluated the actin-binding activity of Ain1 using the recombinant protein. We also investigated the cellular localization of Ain1 and mutant proteins and elucidated the intra-molecular mechanisms underlying the CR-limited localization of Ain1. Our results indicate an elaborate mechanism involving Ain1 in the binding of F-actin in the CR.

Materials and Methods

Yeast strains and cell culture

We used *S. pombe* wild-type (h^- *leu1-32*) and *Δain1* (h^- *leu1-32 ain1::kan*^{r}) strains in this study. In order to observe the actin cytoskeleton, we used a strain that expressed a LifeAct peptide (*32*) fused with a four tandem repeat of the fluorescent protein mCherry (h^- *ura4-D18 ade6-M216*$^+$ *leu1::cdc4-promoter-lifeact-4×mCherry*) (*33*). According to the method described by Forsburg and Rhind (*34*), rich medium YE and minimal medium EMM with supplements were used for cell cultures. In microscopic observations, cells were cultured in EMM liquid medium at 30°C to the log growth phase.

Protein Purification

The *ain1*$^+$ gene was artificially synthesized and cloned in a bacterial plasmid (see Fig. S1) because our attempts to clone any cDNA encoding an entire region of the open reading frame (ORF) were unsuccessful. The codon usage of artificially synthesized cDNA was modified for the efficient translation of the gene product in *Escherichia coli* and *S. pombe*. After plasmid DNA was digested with *Eco*RI and *Sal*I, electrophoretically separated 1.2-kb DNA fragments covering the ORF of *ain1*$^+$ were extracted from agarose gel and inserted into pGEX6P-1 (GE Healthcare (GE)). In order to prepare truncated or point-mutated recombinant proteins (Table S1), the *ain1*$^+$ gene on the vector, pGEX6P-ain1, was modified using the PrimeSTAR® mutagenesis basal kit (Takara). *E. coli* strains, *XL1-Blue*, *BL21*, or Rosetta-gami (DE3) pLysSRARE2 (Takara) were transformed with the resultant vectors, and N-terminal glutathione *S*-transferase (GST)-tagged proteins were expressed according to the manufacturer's protocol (GE).

Bacterial cells expressing the recombinant proteins were lysed by sonication in 50 mM Tris-HCl (pH 8.0) containing 100 mM NaCl, 0.5% NP-40, 1 mM DTT, and protease inhibitors (2 mM PMSF and 1 μg/mL Pepstatin A) on ice, and the cell lysate was centrifuged (10,000×*g*, 10 min) to remove cell debris. The supernatant was incubated with Glutathione Sepharose 4B beads (GE) for the affinity purification of GST-fusion proteins at 4°C for 18 h. The proteins that bound to the

beads were cleaved by PreScission Protease (GE) in 50 mM Tris-HCl (pH 6.8) containing 150 mM NaCl, 1 mM DTT, and 1 mM EDTA on ice. The eluted final product was collected and stored at -80ºC. Before being examined, thawed proteins were centrifuged (200,000×*g*, 10 min) to remove aggregates.

G-actin from rabbit skeletal muscle was purified in our lab as described previously (*27*) or an equivalent product was kindly provided by Prof. Uyeda's lab (National Institute of Advanced Industrial Science and Technology, Japan (AIST)). Some experiments were performed using chicken skeletal muscle actin instead of rabbit skeletal muscle actin. Their primary sequences were identical. G-actin was dissolved in KMEI buffer (100 mM KCl, 1 mM Mg_2Cl, 0.2 mM EGTA, 0.2 mM DTT, 0.2 mM ATP, and 100 mM imidazole-HCl (pH 7.5)) to prepare F-actin.

Purified proteins used in this study are shown in Fig. 1A.

Co-sedimentation assay

F-actin with various concentrations of Ain1 or Ain1ABD was incubated in KMEI at 25ºC for 30 min. In the bundling assay with Ca^{2+} ions, $CaCl_2$ was added at a final concentration of 0.2 mM to the reaction solution in consideration of the concentrations of Ca^{2+} chelators and salts. The mixtures were centrifuged at 200,000×*g* for 20 min (high-speed) or at 15,000×*g* for 15 min (low-speed). The supernatants and pellets were separated by SDS-PAGE, and gels were stained with Coomassie brilliant blue (CBB). CBB-stained gels were scanned as digital images in order to quantify the concentrations of actin and Ain1 using ImageJ 1.47 (National Institutes of Health, USA). Apparent dissociation constants (K_d) were calculated for F-actin from hyperbolic curves fit to the plot of [protein bound to F-actin] versus [protein free] using R (http://www.R-project.org/).

Actin-bundling assay

Dried rhodamine-phalloidin (Molecular Probes) in a microtube was dissolved in KMEI buffer, and F-actin was labeled overnight in the microtube. Labeled F-actin (4 μM) and Ain1 or Ain1-mutant proteins (8 μM) were mixed and incubated at 25ºC for 10 min. The fluorescence microscope BX51

(Olympus) with a PlanApo 100x/1.40 NA objective lens (Olympus) was used for observations. Microscopic images were obtained by ORCAII-ER-1394, the cooled charge-coupled device (CCD) camera, (Hamamatsu Photonics) with the software Simple PCI (Compix Inc.).

Cellular localization of Ain1 and mutant proteins

The thiamine-repressible expression vector pREP1 (*35*) was used for the expression of the N-terminal yellow-fluorescence protein (YFP)-tagged Ain1 and mutant proteins in *S. pombe* (Table S1). Truncated or point mutated genes were prepared using the PrimeSTAR® mutagenesis basal kit (Takara). Cells were transformed with vectors using the lithium acetate method (*36*). SD medium (Becton, Dickinson and Company) was conveniently used as a minimal medium for the first auxotrophic selection of transformants. EMM medium with (repressed condition of the inserted gene) or without (induced condition) 5 μM thiamine was used for microscopic observations of cells.

Cell images were acquired with the fluorescence microscopy system described above. Prior to measuring the florescence intensity of YFP-tagged proteins using ImageJ 1.47 software, mean background intensity was subtracted from the images acquired. Cytoplasmic areas, avoiding nuclei, were arbitrarily selected. Lines with a width of 3 pixels (0.19 μm) were drawn on the CR and the average intensity of two peaks was measured for each cell.

Results

Ain1 binds weakly to F-actin

We measured the actin-binding activity of the full-length molecule of Ain1 (Ain1FL) using a co-sedimentation assay. F-actin predominantly accumulated in pellets with ultracentrifugation (Fig. 1B, bottom panel). On the other hand, Ain1FL alone was detected in the supernatant; however, this molecule was also detected in the pellet fraction under our experimental conditions (Fig. 1B, upper panel). Although the reason for this remains unclear, Ain1FL has been suggested to adhere to the internal walls of centrifuge tubes. By mixing Ain1FL with F-actin, the proportion of Ain1FL in the pellet fraction increased (Fig. 1B, bottom panel). This result indicates that Ain1FL possesses F-actin-binding activity. We then estimated the K_d of Ain1FL (Ain1FL, 6.53 ± 0.55; mean ± standard deviation (SD)) (Fig. 1C); however, the saturated binding ratio of Ain1 to F-actin was not accurately measured. This apparent K_d was similar to the value of 4.3 μM reported by Li and colleagues (*31*). In fission yeast, the K_d of three other actin-binding proteins were as follows; Stg1, 4.4 μM (*16*); Rng2CHD, 0.21 ± 0.08 μM (*27*); Fim1, 0.645 ± 0.15 μM (*37*). Regarding the K_d of Rng2CHD, Tebbs and Pollard recently obtained a 100-fold higher K_d, 20 μM (*28*). They indicated that the lower K_d in a previous study (*27*) may have been an artifact of the effect of a His tag that was not removed from recombinant Rng2CHD. On the other hand, Uyeda and his colleagues independently purified Rng2CHD and measured its K_d against F-actin after removing a His tag from the recombinant protein. Their measured value was 0.42 μM (our personal communication). Thus, Ain1 appears to be an actin-binding protein with relatively low affinity to F-actin in *S. pombe*. It should be noted that all of the measurements cited above and this study have been performed with actin purified from vertebrate skeletal muscle but not *S. pombe* cells.

We next attempted to assess the biochemical activity of the ABD in the N terminus of Ain1. The ratios of the truncated protein Ain1ABD in a pellet did not significantly change with or without F-actin (Fig. 1D), suggesting that Ain1ABD hardly bound to F-actin. We discussed the reason for this later.

Ain1 bundles F-actin independently of Ca^{2+} ions

The actin-bundling activity of Ain1 was examined. F-actin formed thick and long bundles in the presence of Ain1FL, but not Ain1ABD (Fig. 2A). In addition, F-actin with Ain1FL, but not F-actin alone dominantly appeared in the pellet fraction after low-speed centrifugation (Fig. 2B). These results demonstrated that Ain1 exhibits actin-bundling activity *in vitro*. Moreover, a significant amount of F-actin was found in the pellets also at relatively lower concentrations of Ain1FL (Fig. 2C) even though the actin-binding affinity of Ain1FL was not so high as mentioned before (*see* Fig. 1C), suggesting that F-actin could be effectively precipitated at low degree of crosslinking in this assay. On the other hands, Ain1ABD did not exhibit actin-bundling activity in the same condition (Fig. 2A, C).

The EF-hand is the representative Ca^{2+}-binding motif of eukaryotic proteins (*38*). A structural analysis revealed that the C-terminal EF-hand of α-actinin was adjacent to the N-terminal ABD of the paired molecule in a dimer of α-actinin (*39*). In addition, several types of α-actinin including mammalian isoforms 1 and 4 expressed in non-muscle tissues have been shown to exhibit Ca^{2+}-sensitive actin-binding activity (*40*). The interaction between the EF-hand motif and ABD regulates the actin-binding activity of α-actinin. A low-conservative EF-hand was detected in Ain1, but may be insensitive to Ca^{2+} ions (*25*). In order to assess the effects of Ca^{2+} ions on the actin-bundling activity of Ain1, we performed a low-speed co-sedimentation assay (Fig. 2C). The results obtained showed that Ca^{2+} ions did not significantly affect the actin-bundling activity of Ain1.

Three actin-binding sites of Ain1 may have different roles in a cell

The ABD of α-actinin consists of two-tandem CHDs. The N-terminal CHD (CH1) contains two actin-binding sites, ABS1 and ABS2, whereas the other CHD (CH2) has a single site, ABS3 (*41–43*). In dividing *S. pombe* cells, Ain1 specifically localizes to the CR in a manner that depends on F-actin (*25*). We investigated the cellular localization of YFP-tagged Ain1-truncated proteins in wild-type cells in order to characterize the roles of two CHDs in Ain1 in a cell (Fig. 3A). Consistent

with biochemical activity, Ain1ABD did not localize to any structures known as the actin cytoskeleton (Fig. 3A). On the other hand, CH1 had the ability to localize to the CR (Fig. 3A, S3). However, the cellular localization of CH1 appeared to be abnormal because several cortical dots and cables were detected besides the medial ring. Most of these excrescent structures were not labeled with lifeact-4×mCherry, which was used as a marker for F-actin structures (Fig. S3). CH1 and the Lifeact peptide may bind to F-actin in a competitive manner (*44*). Moreover, the overproduction of CH1 induced the formation of thick actin fibers that were significantly resistant to the actin-polymerization inhibitor, Latrunculin-A (Fig. S4). Therefore, CH1 may bind to F-actin in the actin cytoskeleton of a cell; however, this appeared to affect its organization and dynamics. On the other hand, CH2 was not observed in any actin structures (Fig. 3A). We speculated that CH2 retained actin-binding activity because Ain1ΔCH1, the N-terminal truncated Ain1 that lacks CH1, remained localized to the CR, although its activity appeared to be significantly weaker than that of Ain1FL (Fig. 3A). Moreover, a point mutation in ABS3 abolished the CR localization of Ain1ΔCH1 (see below), and neither Ain1ΔABD nor Ain1EF localized to the CR (Fig. 3A). In addition, the overexpression of Ain1ΔCH1 produced elongated cells with multiple nuclei, possibly as a result of interfering with the actin cytoskeletal organization during cytokinesis (Fig. 3B), which is reminiscent of the defect in cytokinesis caused by the overexpression of Ain1FL (*25*). Taken together, both CHDs in Ain1 appear to have the ability to bind to F-actin in a living cell, but may exhibit different activities. We then attempted to assess their biochemical activities, but were unsuccessful because their corresponding functional recombinant proteins were not available as they were insoluble (data not shown).

As described above, we were unable to clearly detect the actin-binding activity of Ain1ABD *in vitro* and *in vivo*, which suggests that CH1 and CH2 mutually affect each other in a suppressive manner. In *H. sapiens* α-actinin ACTN4, the single point mutation that substitutes the lysine residue at 225 with glutamate causes a change in the configuration of two CHDs and increases affinity to F-actin (*42*). We examined the K_d of Ain1 R216E that possessed a mutation presumably equivalent to the K225E mutation in ACTN4, against F-actin, and estimated it to be 1.80 ± 0.47 (mean ± SD),

suggesting that the substitution of the single amino acid residue greatly increased the actin-binding activity of Ain1 (Fig. 1C). In addition, it was found that Ain1 R216E bundled F-actin (Fig. 2A) although the activity was somewhat weak as compared with the wild-type Ain1FL at the lower concentrations of those proteins to actin (Fig. 2C). We also found that although Ain1 R216E proteins encircled the middle region of mitotic cells, the ring shape was deformed (Fig. 3A, S3). This phenotype resembled the abnormal organization of the CR in Ain1-overproducing cells (*29*). Independent of this study, Li et al. recently reported that the formation and constriction of the CR were affected by the R216E mutation in *ain1*$^{+}$ (*31*). In order to compare the accumulation of Ain1R216E with the wild-type Ain1, Ain1FL, in the middle of the cell, the intensities of these YFP-fusion proteins were quantified (Fig. 3C). The accumulation of Ain1R216E in the cell middle (7.39 ± 3.01, mean ± SD) was approximately 2-fold greater than that of Ain1FL (3.78 ± 0.92). These results suggest that the structural interaction between CH1 and CH2 moderates the actin-binding activity of Ain1 in a similar manner to ACTN4 (*42*). However, the introduction of the R216E mutation did not restore the actin cytoskeleton-binding activity of the ABD *in vivo* (*see* Ain1ABD R216E in Fig. 3A). Therefore, the dimerization of protein or the intra- or inner-molecular interaction of the ABD with another part of Ain1 may be important for the actin-binding activity of the full-length molecule.

We also investigated the functional relationship of each ABS using the point mutations, ABS1-2A, ABS2-1A, and ABS3-2A (*see* Fig. 6A, Table S1). These mutations substitute the charged amino acid(s) to alanine in the corresponding ABS. The ABSs of Ain1 were deduced from the alignment of the primary sequence of Ain1 with the human skeletal muscle α-actinin ACTN3 and *S. pombe* fimbrin (41, 43). ABS1-2A did not significantly affect the cellular localization of the full-length protein or truncated CH1 domain (Fig. 3A), whereas the corresponding mutation significantly reduced the actin-binding activity of ACTN4 (42). In contrast, ABS2-1A abolished the CR localization of the full-length protein (Fig. 3A). Moreover, CH1 with the ABS2-1A mutation did not display marked cellular localization (Fig. 3A). Therefore, ABS2 appears to be the major actin-binding site of Ain1 in *S. pombe* cells. However, the importance of ABS1 and ABS2 in the

cellular localization of Ain1 was affected by the R216E mutation. Ain1 containing the ABS2-1A mutation simultaneously with R216E localized to the CR, whereas Ain1 containing ABS1-2A and R216E did not (Fig. 3A). Therefore, the R216E mutation may induce a steric conformational change in the CH1 domain. On the other hand, Ain1ΔCH1 with the ABS3-2A mutation lost its localization to the CR, suggesting that ABS3 is the sole actin-binding site in the CH2 domain (Fig. 3A). Furthermore, Ain1 ABS3-2A localized not only to the CR, but also cortical dots (Fig. 3A); however, excrescent dot-like localization was not observed in cells co-expressing Lifeact-4×mCherry presumably because of their competitive binding to F-actin (Fig. S3). Thus, ABS3 appears to play an important role in the CR-specific localization of Ain1.

We then evaluated the cell growth abilities of *ain1*-null cells expressing each Ain1 mutant protein under stress conditions. At 18°C in the presence of 1 M potassium chloride, a condition described previously (*25*), *ain1*-null cells expressing Ain1ABS3-2A grew as well as wild-type cells and *ain1*-null cells expressing Ain1FL (Fig. 4). This result suggested that Ain1ABS3-2A was able to function as well as the wild-type Ain1FL *in vivo* even though it localizes to other actin structures besides CR. Thus, CR-limited localization of Ain1 is not essential for cytokinesis. On the other hand, neither the expression of Ain1 ABS1-2A nor Ain1 ABS2-1A restored growth defects in *ain1*-null cells under the same conditions. Therefore, not only ABS2, but also ABS1 may be required for the binding of Ain1 to F-actin in the CR. In support of this, Ain1 ABS1-2A was excluded from the CR when Lifeact-4×mCherry was simultaneously expressed (Fig. S3). On the other hand, the truncated CH1 domain with the ABS1-2A mutation still localized to the F-actin structure (Fig. S3).

The C-terminal region is required for the cellular localization of Ain1

In the course of our study on the cellular localization of truncated Ain1 proteins, we found that Ain1 lacking the C-terminal region, Ain1ΔEF, did not localize to the CR (Figs. 3A, S5B). The expression level of Ain1ΔEF was similar to that of the wild-type protein in control cells (Fig. S5A, C). Coincidentally, the expression of Ain1ΔEF from the plasmid failed to rescue the growth defect in

ain1-null cells under stress conditions (Fig. 4). A previous study suggested that the actin-binding activity of mammalian α-actinin is controlled by the C-terminal region, containing an EF-hand motif, of the paired molecule in the dimer (*45*). Similarly, the intersubunit interaction between the N-terminal ABD and C-terminal region may be required for the actin-binding activity of Ain1 in *S. pombe* cells. Ain1ΔEF containing the R216E mutation localized to the medial ring and cortical dots (Figs. 3A, S3). Therefore, the C-terminal region of Ain1 may positively function in the actin binding of the paired molecule in the α-actinin dimer by controlling conformational changes in the ABD. The results of biochemical experiments showed that Ain1ΔEF bound F-actin with a slightly higher affinity than Ain1FL; the apparent K_d of Ain1ΔEF with F-actin was 4.92 ± 1.08 (mean ± SD) (Fig. 1C). Moreover, Ain1ΔEF induced the formation of actin bundles *in vitro* (Fig. 2A, C). Therefore, the C-terminal region of Ain1 is not essential for actin binding *in vitro*, but is important *in vivo*.

Investigation of the role of PIP_2 in the cellular localization of Ain1

Phosphatidylinositol 4,5-bisphosphate (PIP_2) has been identified as a regulatory molecule of α-actinin. α-actinin has a single PIP_2-binding site (*46*), and PIP_2 enhances the formation of F-actin gels induced by α-actinin (*47*). A previous study reported that the putative PIP_2 binding-site in Ain1 had 47 % identity with chicken skeletal-muscle α-actinin (*25*). In addition, PI (4) P-5-kinase Its3 and the product PIP_2 were both present in the division site in *S. pombe* (*48*). We then investigated whether Its3 is required for the localization of Ain1 in the middle of mitotic cells. However, Ain1 was still localized there in *its3* mutant cells, even at the restrictive temperature 36ºC (Fig. 5). Therefore, PIP_2 is unlikely to regulate the mitotic-specific interaction of Ain1 with F-actin in the CR.

Discussion

Ain1 may ensure actin dynamics of F-actin bundles in the CR

We herein biochemically demonstrated that Ain1 exhibited actin-bundling activity, whereas it bound to F-actin with lower affinity than other actin-bundling proteins previously studied in *S. pombe*. The mechanisms underlying cytokinesis in fission yeast have been examined in detail. The SCPR model represents one of the convincing theories for the formation of the CR from nodes (*49*). *S. pombe* cells have approximately 50–60 nodes consisting of CR-precursor proteins in the cell middle before mitosis (*50*). After G2/M transition, each node recruits myosin II and formin, an actin-polymerizing protein essential for CR formation, and F-actin newly polymerized from each node connects them into a single network. The interaction of F-actin and myosin II between each node induces their redistribution together with their associated proteins, and the equatorial actomyosin network finally forms a ring. Ain1 has been suggested to subserve a function in CR formation from nodes by cross-linking the F-actin network (*29*). Moreover, Ain1 may bundle F-actin in the CR in order to ensure the maintenance of the ring shape after its formation. A previous study demonstrated that mammalian α-actinin, which is involved in cytokinesis, shows a high affinity for F-actin (K_d = 0.20 ± 0.01 μM) (*51*). On the other hand, the extremely low affinity of Ain1 to F-actin indicates that Ain1 is unlikely to bundle F-actin stably. Differences in the α-actinin-mediated F-actin-bundling activity in the CR between mammalian cells and fission yeast cells may be attributed to the sizes of their CRs. In addition, mammalian α-actinin has been shown to decelerate the constriction rate of the CR (*26*). On the other hand, the constriction rate of the CR is not changed with or without Ain1 (*29*), suggesting that Ain1 is an actin cross-linker that does not affect actin dynamics in the CR. The point mutation R216E resulted in the prominent accumulation of Ain1 in the cell middle (Fig. 3C). The excessive F-actin-binding activity of Ain1 may deform the ring shape of the CR, which is consistent with the findings of computational simulations performed previously (*29*). In proper cytokinesis in fission yeast, Ain1 may ensure the dynamic constriction of the CR by weakly bundling F-actin in the CR.

Mechanism of the CR-specific localization of Ain1

Fission yeast has three types of actin structures (*i.e.* actin patches, actin cables, and the CR). Ain1 specifically localizes to the CR in a manner that is dependent on F-actin, as demonstrated previously (*25*). The spatial and temporal regulatory mechanisms underlying the localization of Ain1 have not yet been elucidated. In mammalian cells, the actin-binding activity of α-actinin decreases with Ca^{2+}, and Ca^{2+} sensitivity is required for the accumulation of α-actinin in the cleavage furrow (*52*). In contrast, the results of our *in vitro* experiment indicated that Ca^{2+} does not inhibit the actin-bundling activity of Ain1 (Fig. 2C). On the other hand, Ain1ΔEF did not localize to any actin structures *in vivo*. A recent structural study on mammalian α-actinin identified an interaction between the EF-hand with the ABD (*45*) and the neck region connecting the ABD to SRs (*39*). Regardless of Ca^{2+} insensitivity, the C-terminal region including the EF-hand in Ain1 may be necessary for maintaining the functional dimer form of Ain1 with actin-binding activity. However, Ain1ΔEF bundled F-actin *in vitro* (Fig. 2A, C). Thus, the C-terminal region-dependent regulation of Ain1 may exert a strong influence on F-actin undergoing a dynamic turnover and interacting with various types of actin-modulating proteins *in vivo*. In future studies, it may be important to investigate whether the structure and function of the C-terminal region are controlled by cell cycle machinery.

We successfully demonstrated the functional diversity of CH1 and CH2 in Ain1 using truncated and point mutated genes (Figs. 3A, 4). In a cell, CH1 localizes to the CR and other types of actin structures in a manner that may be mediated by the interaction of ABS2 with F-actin (Fig. 6). The non-selective association of CH1 with the actin cytoskeleton resembles the case of Rng2. The corresponding truncated protein, Rng2CHD, localizes not only to the CR, but also to other actin cytoskeletons including actin cables and actin patches (*27*). In Rng2, the C-terminal region adjacent to the CHD appears to play an important role in the recognition of F-actin in the CR because Rng2Ns consists of the CHD and the subsequent short region specifically localizes to CR, similar to the full-length protein. On the other hand, our results suggest that CH2 plays a critical role in specific targeting of Ain1 to the CR (Figs. 3A, 6). Therefore, the actin-binding property of CH1

may be modulated by the adjacent CH2. Coincidently, structural studies have indicated a regulatory interaction between CH1 and CH2 in mammalian α-actinin (*41*). The ABD of *S. pombe* Ain1 was also shown to form a similar structure (*30*). The R216E mutation, corresponding to the single point mutation *H. sapiens* α-actinin ACTN4 that causes a configurational change in two CHDs (*42*), caused the prominent accumulation of Ain1 in the middle region of mitotic cells, possibly by abrogating the interaction between CH1 and CH2 (*31*; Fig. 3C). However, the steric behaviors of CH1 and CH2 in the ABD of Ain1 have not yet been elucidated. Their interaction with the C-terminal region of the paired molecule may also be important. A role-sharing relationship between CHDs in the ABD may generally be conserved in α-actinin proteins because fungal α-actinin is considered to be a prototype of animal α-actinin proteins (*53*).

As discussed above, we successfully demonstrated that CH2 plays a critical role in the CR-specific localization of Ain1. CH2 may favor actin structures decorated with CR-specific actin-binding proteins. Previous studies demonstrated that the N-terminal-acetylated Cdc8, the sole tropomyosin homologue in *S. pombe*, specifically localized to the CR (*54*, *55*). The preference of CH2 for F-actin with acetylated Cdc8 warrants further study. In addition, actin-binding proteins may not only collaboratively but also competitively modulate their localization on the actin cytoskeleton. In *S. pombe*, Fim1 has been shown to dominantly localize to actin patches (*24*, *25*). Fim1 and Ain1 both bind to F-actin via their ABDs, and Fim1 has markedly higher affinity to F-actin than Ain1, as described above (*31, 56*, this study). Therefore, Fim1 may competitively exclude Ain1 from actin patches and confine Ain1 to interact with F-actin in the CR.

Acknowledgments

We are deeply grateful to Prof. Uyeda and Dr. Yamada (AIST) for providing us with purified actin and for their valuable advice. This work was supported by a Grant-in-Aid for Scientific Research to K.N. from the Ministry of Education, Culture, Sports, Science and Technology (MEXT) [24570207].

References

1. Pollard, T.D. and Wu, J.Q. (2010) Understanding cytokinesis: lessons from fission yeast. *Nat. Rev. Mol. Cell Biol.* **11**, 149–155.
2. Goyal, A., Takaine, M., Simanis, V., and Nakano, K. (2011) Dividing the spoils of growth and the cell cycle: the fission yeast as a model for the study of cytokinesis. *Cytoskeleton* **68**, 69–88.
3. Rozenblum GT. and Gimona M. (2007) Calponins: adaptable modular regulators of the actin cytoskeleton. *Int. J. Biochem. Cell Biol.* **40**, 1990–1995.
4. Gimona, M., Djinovic-Carugo, K., Kranewitter, W.J., and Winder, S.J. (2002) Functional plasticity of CH domains. *FEBS Lett.* **513**, 98–106.
5. Korenbaum, E. and Rivero, F. (2002) Calponin homology domains at a glance. *J. Cell Sci.* **115**, 3543–3545.
6. Bashour, A.M., Fullerton, A.T., Hart, M.J., and Bloom, G.S. (1997) IQGAP1, a Rac- and Cdc42-binding protein, directly binds and cross-links microfilaments. *J. Cell Biol.* **137**, 1555–1566.
7. Mateer, S.C., Morris, L.E., Cromer, D.A., Benseñor, L.B., and Bloom, G.S. (2004) Actin filament binding by a monomeric IQGAP1 fragment with a single calponin homology domain. Cell Motil. *Cytoskeleton* **58**, 231–241.
8. Shannon, K.B. and Li, R. (1999) The multiple roles of Cyk1p in the assembly and function of the actomyosin ring in budding yeast. *Mol. Biol. Cell* **10**, 283–296.
9. Wang, S., Watanabe, T., Noritake, J., Fukata, M., Yoshimura, T., Itoh, N., Harada, T., Nakagawa, M., Matsuura, Y., Arimura, N., and Kaibuchi, K. (2007) IGAP3, a novel effector of Rac1 and Cdc42, regulates neurite outgrowth. *J. Cell Sci.* **120**, 567–577.
10. Watanabe, T., Wang, S., and Kaibuchi, K. (2015) IQGAPs as key regulators of actin-cytoskeleton dynamics. *Cell Struct. Funct.* **40**, 69–77.
11. Nishimura, Y. and Mabuchi, I. (2003) An IQGAP-like protein is involved in actin assembly together with Cdc42 in the sea urchin egg. *Cell Motil. Cytoskeleton* **56**, 207–218.

12. Bielak-Zmijewska, A., Kolano, A., Szczepanska, K., Maleszewski, M., and Borsuk, E. (2008) Cdc42 protein acts upstream of IQGAP1 and regulates cytokinesis in mouse oocytes and embryos. *Dev. Biol.* **322**, 21–32.

13. Adachi, M., Kawasaki, A., Nojima, H., Nishida, E., and Tsukita, S. (2014) Involvement of IQGAP family proteins in the regulation of mammalian cell cytokinesis. *Genes Cells* **19**, 803–820.

14. Epp, J.A. and Chant, J. (1997) An IQGAP-related protein controls actin-ring formation and cytokinesis in yeast. *Curr. Biol.* **7**, 921–929.

15. Eng, K., Naqvi, N.I., Wong, K.C., and Balasubramanian, M.K. (1998) Rng2p, a protein required for cytokinesis in fission yeast, is a component of the actomyosin ring and the spindle pole body. *Curr. Biol.* **8**, 611–621.

16. Nakano, K., Bunai, F., and Numata, O. (2005) Stg1 is a novel SM22/transgelin-like actin-modulating protein in fission yeast. *FEBS Lett.* **579**, 6311–6316.

17. Stossel, T.P., Condeelis, J., Cooley, L., Hartwig, J.H., Noegel, A., Schleicher, M., and Shapiro, S.S. (2001) Filamins as integrators of cell mechanics and signalling. *Nat. Rev. Mol. Cell Biol.* **2**, 138–145.

18. Nunnally, M.H., D'Angelo, J.M., and Craig, S.W. (1980) Filamin concentration in cleavage furrow and midbody region: frequency of occurrence compared with that of alpha-actinin and myosin. *J. Cell Biol.* **87**, 219–226.

19. Szeto, S.G.Y., Williams, E.C., Rudner, A.D., and Lee, J.M. (2015) Phosphorylation of filamin A by Cdk1 regulates filamin A localization and daughter cell separation. *Exp. Cell Res.* **330**, 248–266.

20. Faix, J., Steinmetz, M., Boves, H., Kammerer, R.A., Lottspeich, F., Mintert, U., Murphy, J., Stock, A., Aebi, U., and Gerisch, G. (1996) Cortexillins, major determinants of cell shape and size, are actin-bundling proteins with a parallel coiled-coil tail. *Cell* **86**, 631–642.

21. Liu, X., Shu, S., Yu, S., Lee, D.Y., Piszczek, G., Gucek, M., Wang, G., and Korn, E.D. (2014) Biochemical and biological properties of cortexillin III, a component of *Dictyostelium* DGAP1-cortexillin complexes. *Mol. Biol. Cell* **25**, 2026–2038.

22. Stock, A., Steinmetz, M.O., Janmey, P.A., Aebi, U., Gerisch, G., Kammerer, R.A., Weber, I., and Faix, J. (1999) Domain analysis of cortexillin I: actin-bundling, PIP_2-binding and the rescue of cytokinesis. *EMBO J.* **18**, 5274–5284.

23. Watanabe, A., Kurasawa, Y., Watanabe, Y., and Numata, O. (1998) A new *Tetrahymena* actin-binding protein is localized in the division furrow. *J Biochem* **123**, 607–613.

24. Nakano, K., Satoh, K., Morimatsu, A., Ohnuma, M., and Mabuchi, I. (2001) Interactions among a fimbrin, a capping protein, and an actin-depolymerizing factor in organization of the fission yeast actin cytoskeleton. *Mol. Biol. Cell* **12**, 3515–3526.

25. Wu, J.Q., Bähler, J., and Pringle, J.R. (2001) Roles of a fimbrin and an alpha-actinin-like protein in fission yeast cell polarization and cytokinesis. *Mol. Biol. Cell* **12**, 1061–1077.

26. Mukhina, S., Wang, Y.L., and Murata-Hori, M. (2007) α-actinin is required for tightly regulated remodeling of the actin cortical network during cytokinesis. *Dev. Cell* **13**, 554–565.

27. Takaine, M., Numata, O., and Nakano, K. (2009) Fission yeast IQGAP arranges actin filaments into the cytokinetic contractile ring. *EMBO J.* **28**, 3117–3131.

28. Tebbs, I.R. and Pollard, T.D. (2013) Separate roles of IQGAP Rng2p in forming and constricting the *Schizosaccharomyces pombe* cytokinetic contractile ring. *Mol. Biol. Cell* **24**, 1904–1917.

29. Laporte, D., Ojkic, N., Vavylonis, D., and Wu, J.Q. (2012) α-actinin and fimbrin cooperate with myosin II to organize actomyosin bundles during contractile-ring assembly. *Mol. Biol. Cell* **23**, 3094–3110.

30. Addario, B., Sandblad, L., Persson, K., and Backman, L. (2016) Characterisation of *Schizosaccharomyces pombe* α -actinin. *PeerJ* **4**, e1858.

31. Li, Y., Christensen, J.R., Homa, K.E., Hocky, G.M., Fok, A., Sees, J.A., Voth, G.A., and Kovar, D.R. (2016) The F-actin bundler α-actinin Ain1 is tailored for ring assembly and constriction during cytokinesis in fission yeast. *Mol. Biol. Cell* **27**, 1821–1833.

32. Riedl, J., Crevenna, A.H., Kessenbrock, K., Yu, J.H., Neukirchen, D., Bista, M., Bradke, F., Jenne, D., Holak, T.A., Werb, Z., Sixt, M., and Wedlich-Soldner, R. (2008) Lifeact: a versatile marker to visualize F-actin. *Nat. Methods* **5**, 605–607.

33. Takaine, M., Numata, O., and Nakano, K. (2015) An actin-myosin-II interaction is involved in maintaining the contractile ring in fission yeast. *J. Cell Sci.* **128**, 2903–2918.

34. Forsburg, S.L. and Rhind, N. (2006) Basic methods for fission yeast. *Yeast* **23**, 173–183.

35. Maundrell, K. (1993) Thiamine-repressible expression vectors pREP and pRIP for fission yeast. *Gene* **123**, 127–130.

36. Suga, M. and Hatakeyama, T. (2005) A rapid and simple procedure for high-efficiency lithium acetate transformation of cryopreserved *Schizosaccharomyces pombe* cells. *Yeast* **22**, 799–804.

37. Skau, C.T., Courson, D.S., Bestul, A.J., Winkelman, J.D., Rock, R.S., Sirotkin, V., and Kovar, D.R. (2011) Actin filament bundling by fimbrin is important for endocytosis, cytokinesis, and polarization in fission yeast. *J. Biol. Chem.* **286**, 26964–26977.

38. Strynadka, N.C.J. and James, M.N.G. (1989) Crystal structures of the helix-loop-helix calcium-binding proteins. *Annu. Rev. Biochem.* **58**, 951–999.

39. Ribeiro, E. de A. Jr., Pinotsis, N., Ghisleni, A., Salmazo, A., Konarev, P.V., Schreiner, C., Polyansky, A.A., Gkougkoulia, E.A., Holt, M.R., Kostan, J., Bordignon, E., Pirker, K.F., Svergun, D.I., Gautel, M., Aachmann, F.L., and Zagrovi, B. (2014) Article the structure and regulation of human muscle α-actinin. *Cell* **159**, 1447–1460.

40. Foley, K.S. and Young, P.W. (2014) The non-muscle functions of actinins: an update. *Biochem. J.* **459**, 1–13.

41. Franzot, G., Sjöblom, B., Gautel, M., and Djinović Carugo, K. (2005) The crystal structure of the actin binding domain from alpha-actinin in its closed conformation: structural insight into phospholipid regulation of alpha-actinin. *J. Mol. Biol.* **348**, 151–165.

42. Weins, A., Schlondorff, J.S., Nakamura, F., Denker, B.M., Hartwig, J.H., Stossel, T.P., and Pollak, M.R. (2007) Disease-associated mutant α-actinin-4 reveals a mechanism for regulating its F-actin-binding affinity. *Proc. Natl. Acad. Sci.* **104**, 16080–16085.

43. Klein, M.G., Shi, W., Ramagopal, U., Tseng, Y., Wirtz, D., Kovar, D.R., Staiger, C.J., and Almo, S.C. (2004) Structure of the actin crosslinking core of fimbrin. *Structure* **12**, 999–1013.

44. Courtemanche, N., Pollard, T.D., and Chen, Q. (2016) Avoiding artefacts when counting polymerized actin in live cells with LifeAct fused to fluorescent proteins. *Nat. Cell Biol.* **18**, 676–683.

45. Prebil, S., Slapšak, U., Pavšič, M., Ilc, G., Puž, V., de Ribeiro, E., Anrather, D., Hartl, M., Backman, L., Plavec, J., Lenarčič, B., and Djinović-Carugo, K. (2016) Structure and calcium-binding studies of calmodulin-like domain of human non-muscle α-actinin-1. *Sci Reports* **6**, 27383.

46. Fukami, K., Sawada, N., Endo, T., and Takenawa, T. (1996) Identification of a phosphatidylinositol 4,5-bisphosphate-binding site in chicken skeletal muscle α-actinin. *J. Biol. Chem.* **271**, 2646–2650.

47. Fukami, K., Furuhashi, K., Inagaki, M., Endo, T., Hatano, S., and Takenawa, T. (1992) Requirement of phosphatidylinositol 4,5-bisphosphate for alpha-actinin function. *Nature* **359**, 150–152.

48. Zhang, Y., Sugiura, R., Lu, Y., Asami, M., Maeda, T., Itoh, T., Takenawa, T., Shuntoh, H., and Kuno, T. (2000) Phosphatidylinositol 4-phosphate 5-kinase Its3 and calcineurin Ppb1 coordinately regulate cytokinesis in fission yeast. *J. Biol. Chem.* **275**, 35600–35606.

49. Vavylonis, D., Wu, J.Q., Hao, S., O'Shaughnessy, B., and Pollard, T.D. (2008) Assembly mechanism of the contractile ring for cytokinesis by fission yeast. *Science* **319**, 97–100.

50. Wu, J.Q. and Pollard, T.D. (2005) Counting cytokinesis proteins globally and locally in fission yeast. *Science* **310**, 310–314.

51. Low, S.H., Mukhina, S., Srinivas, V., Ng, C.Z., and Murata-Hori M. (2010) Domain analysis of alpha-actinin reveals new aspects of its association with f-actin during cytokinesis. *Exp. Cell Res.* **316**, 1925–1934.

52. Jayadev, R., Kuk, C.Y., Low, S.H., and Murata-Hori, M. (2012) Calcium sensitivity of α-actinin is required for equatorial actin assembly during cytokinesis. *Cell Cycle* **11**, 1929–1937.

53. Virel, A. and Backman, L. (2007) A comparative and phylogenetic analysis of the alpha-actinin rod domain. *Mol. Biol. Evol.* **24**, 2254–2265.

54. Coulton, A.T., East, D.A., Galinska-Rakoczy, A., Lehman, W., and Mulvihill, D.P. (2010) The recruitment of acetylated and unacetylated tropomyosin to distinct actin polymers permits the discrete regulation of specific myosins in fission yeast. *J. Cell Sci.* **123**, 3235–3243.

55. Johnson, M., East, D.A., and Mulvihill, D.P. (2014) Formins determine the functional properties of actin filaments in yeast. *Curr. Biol.* **24**, 1525–1530.

56. Skau, C.T. and Kovar, D.R. (2010) Fimbrin and tropomyosin competition regulates endocytosis and cytokinesis kinetics in fission yeast. *Curr. Biol.* **20**, 1415–1422.

Legends to figures

Fig. 1 Ain1 binds weakly to F-actin

(A) Purified recombinant proteins used in this study. After being subjected to SDS-PAGE, purities were measured by the densitometry of the CBB-stained gel. **(B)** High-speed co-sedimentation of full-length Ain1 (Ain1FL) (0.25–8 μM) with (bottom) or without F-actin (2 μM) (top). The supernatant (S) and pellet (P) were separated by SDS-PAGE and stained with CBB. **(C)** Plots of free vs. F-actin-bound proteins (Ain1FL, circle; Ain1FL R216E, triangle; Ain1ΔEF, square). Three independent experiments using the high-speed co-sedimentation assay were performed. The average of three experiments is shown with SD (error bar). Each plot was fit to hyperbolic curves. Apparent dissociation constants (K_d) were calculated from each curve. **(D)** High-speed co-sedimentation of the actin-binding domain of Ain1 (Ain1ABD) (2–24 μM) with (bottom) or without (top) F-actin (4 μM). Experiments were performed as in B. Half amounts of the supernatant were applied on lanes with an asterisk.

Fig. 2 Ain1 bundles F-actin independently of Ca^{2+} ions

(A) Fluorescent micrographs of Rhodamine-phalloidin-labeled F-actin incubated with Ain1FL, Ain1ABD, Ain1FL R216E, or Ain1ΔEF. Note that thick actin bundles were formed in the presence of Ain1FL, Ain1FL R216E, and Ain1ΔEF. Images were converted into gray-scale and inverted. **(B)** Low-speed co-sedimentation of F-actin (2 μM) with Ain1FL or Ain1ABD (0.25–2 μM). The supernatant (S) and pellet (P) were separated by SDS-PAGE and stained with CBB. Three independent experiments were performed. Control experiment with Ain1 alone was shown in the supplemental data (Fig. S2). **(C)** Ratios of actin in the pellet fractions estimated from the CBB-stained SDS-PAGE gels in B (mean ± SD, n = 3).

Fig. 3 Cellular localization of Ain1-mutant proteins

(A) Localization of Ain1FL and mutant proteins. Wild-type cells transformed with pREP1-derived vectors containing constructs indicated on the left side were logarithmically grown in EMM with 5

μM thiamine at 30ºC. The cellular localization of N-terminal YFP-tagged proteins was observed. Mitotic cells displaying the representative protein localization were shown. The same result was obtained using *ain1*-null cells (data not shown). Images were converted into gray-scale and inverted. Asterisks indicate point mutation site(s) including R216E, ABS1-3A, ABS2-1A, and ABS3-2A. Arrows and arrowheads indicate the CR and cortical dots, respectively. The bar is 10 μm. **(B)** Overexpression of N-terminal-truncated Ain1 lacking CH1. Wild-type cells containing pREP1YFP-ain1ΔCH1 were incubated as in B without thiamine. Multinucleated cells were frequently observed. **(C)** Ain1FL R216E excessively accumulates in CR. The average intensity of the cytosol and maximum intensity of the CR were measured from a fluorescent micrograph. Data show the ratio of the ring and cytosol (mean ± SD, n > 30). A two-tailed Student's *t*-test was performed assuming unequal variance.

Fig. 4 Functional analysis of Ain1-mutant proteins in cell growth under stress conditions

(A) Wild-type and *ain1*-null cells were transformed with the pREP1-derived vectors indicated above. Cells were incubated on a YE plate at 30°C for 3 days (right) or YE-containing 1M KCl plate at 18°C for one week (left). The viability of cells was indicated; ++, normal sized colonies; +, small colonies; -, no colony.

Fig. 5 Localization of Ain1 in the *its3*-mutant

its3-mutant cells containing pREP1-YFP-ain1FL were incubated at 25°C and shifted to the restrictive temperature of 36°C for 3 h. The bar shows 10 μm.

Fig. 6 Functional relationship of each domain in Ain1

(A) Structural model of the Ain1 ABD (PDBID: 5BVR) (*30*). Two CHDs (right: CH1, left: CH2), three ABSs (black), and four mutation sites are shown. The rotated model (bottom) shows the presumed F-actin binding surface consisting of ABS2 and ABS3. **(B)** Summary of the domain analysis in this study. See the main text for details.

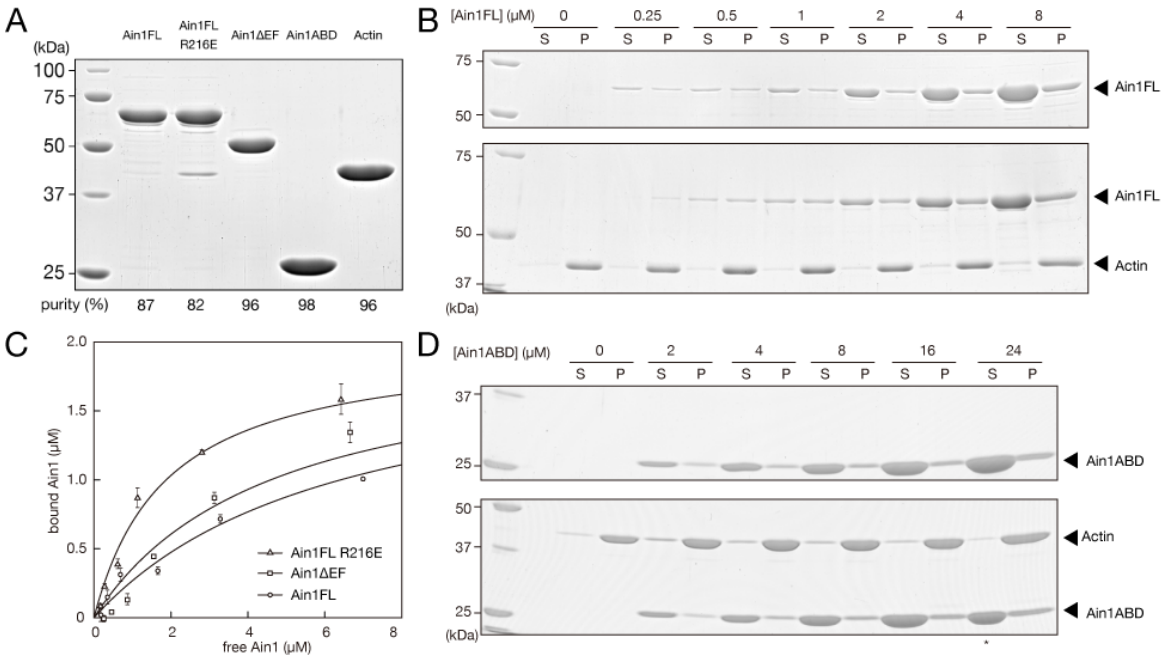
A
(kDa)
Ain1FL
Ain1FL R216E
Ain1ΔEF
Ain1ABD
Actin
100
75
50
37
25
purity (%)
87
82
96
98
96
B
[Ain1FL] (μM)
0
0.25
0.5
1
2
4
8
S P
Ain1FL
Actin
(kDa)
C
bound Ain1 (μM)
free Ain1 (μM)
Ain1FL R216E
Ain1ΔEF
Ain1FL
D
[Ain1ABD] (μM)
0
2
4
8
16
24
Ain1ABD
Actin

Fig. 1

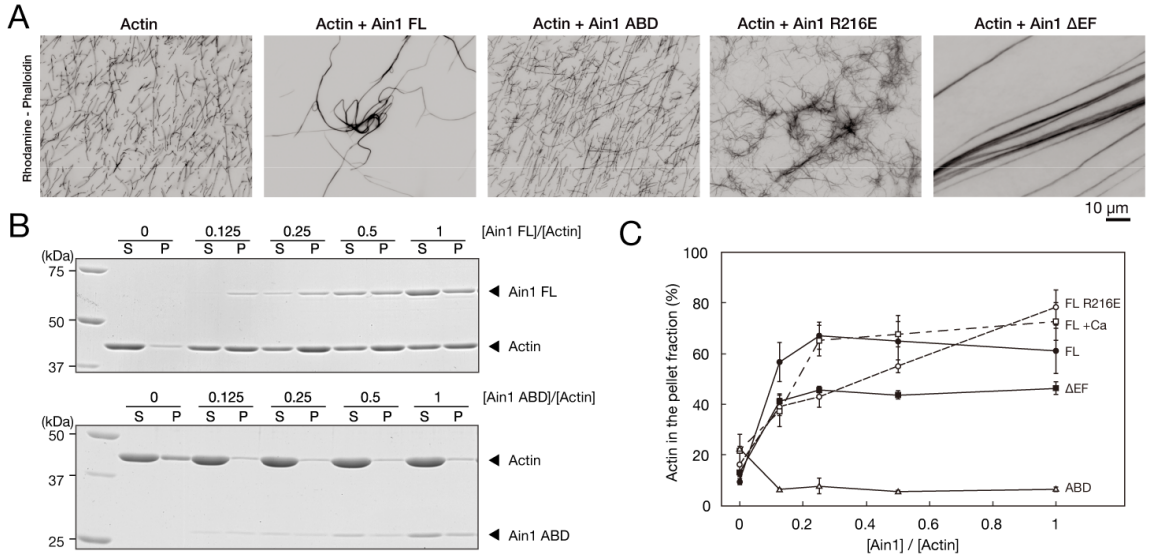
A
Actin
Actin + Ain1 FL
Actin + Ain1 ABD
Actin + Ain1 R216E
Actin + Ain1 ΔEF
Rhodamine - Phalloidin
10 μm
B
0
0.125
0.25
0.5
1
[Ain1 FL]/[Actin]
S P
(kDa)
75
50
37
Ain1 FL
Actin
[Ain1 ABD]/[Actin]
50
37
25
Actin
Ain1 ABD
C
Actin in the pellet fraction (%)
100
80
60
40
20
0
0
0.2
0.4
0.6
0.8
1
[Ain1] / [Actin]
FL R216E
FL +Ca
FL
ΔEF
ABD

Fig. 2

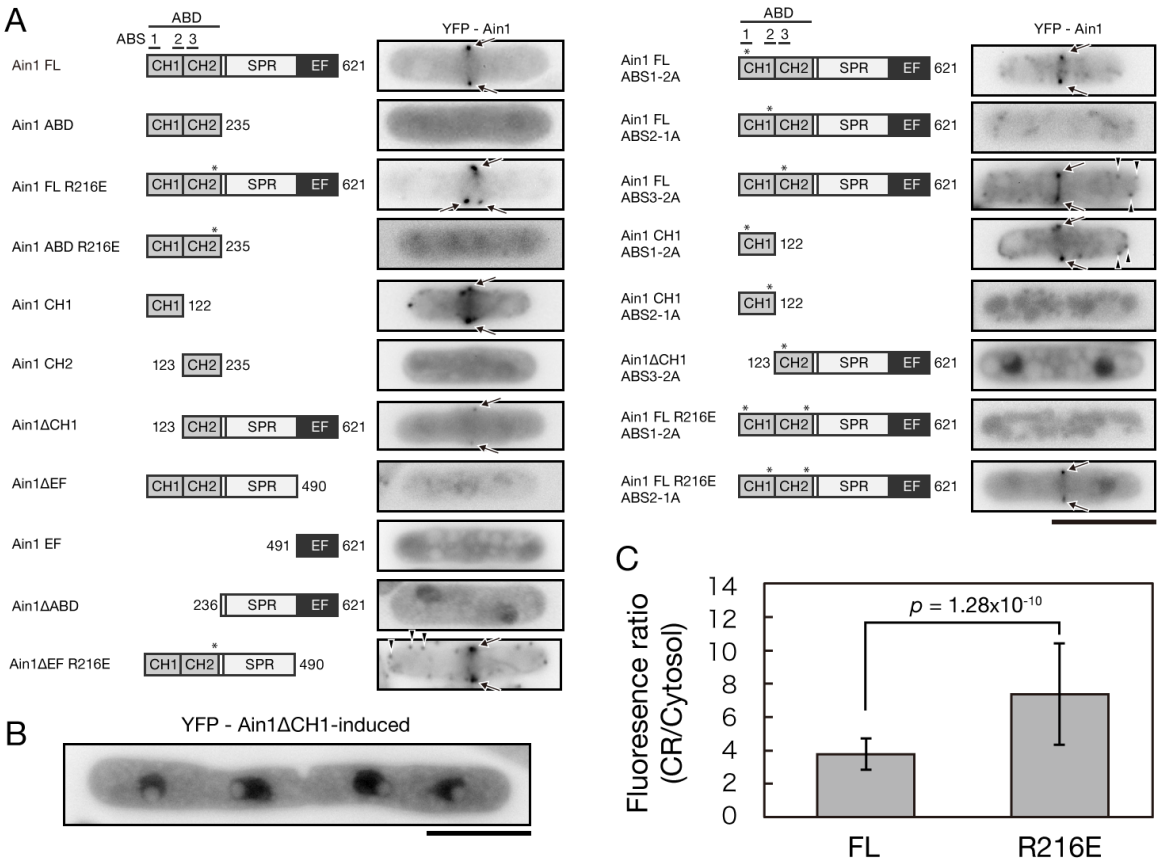
A
ABD
ABS 1 2 3
YFP - Ain1
Ain1 FL
Ain1 ABD
Ain1 FL R216E
Ain1 ABD R216E
Ain1 CH1
Ain1 CH2
Ain1ΔCH1
Ain1ΔEF
Ain1 EF
Ain1ΔABD
Ain1ΔEF R216E
CH1
CH2
SPR
EF
621
235
122
123
236
491
490
Ain1 FL ABS1-2A
Ain1 FL ABS2-1A
Ain1 FL ABS3-2A
Ain1 CH1 ABS1-2A
Ain1 CH1 ABS2-1A
Ain1ΔCH1 ABS3-2A
Ain1 FL R216E ABS1-2A
Ain1 FL R216E ABS2-1A
B
YFP - Ain1ΔCH1-induced
C
Fluoresence ratio (CR/Cytosol)
p = 1.28x10-10
FL
R216E

Fig. 3

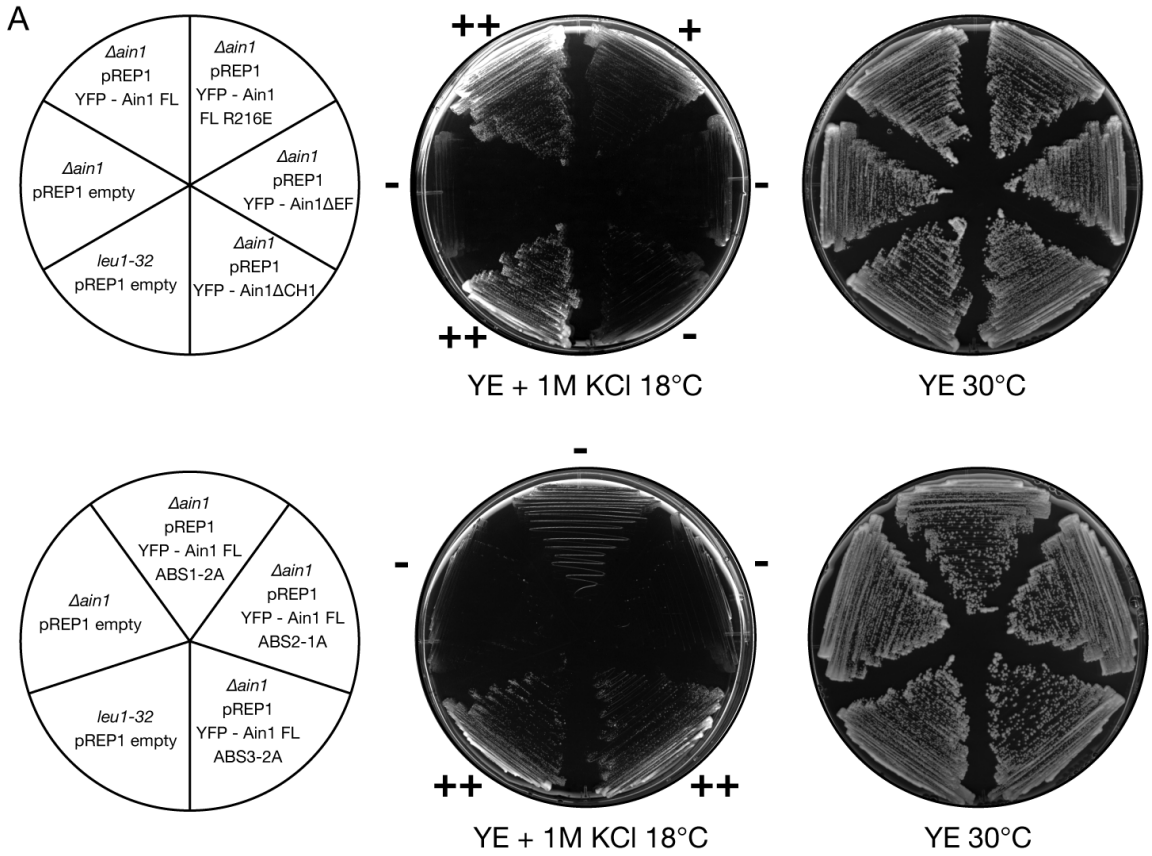
A
Δain1
pREP1
YFP - Ain1 FL
Δain1
pREP1
YFP - Ain1
FL R216E
Δain1
pREP1
YFP - Ain1ΔEF
Δain1
pREP1
YFP - Ain1ΔCH1
leu1-32
pREP1 empty
Δain1
pREP1 empty
++
+
-
-
++
-
YE + 1M KCl 18°C
YE 30°C
Δain1
pREP1
YFP - Ain1 FL
ABS1-2A
Δain1
pREP1
YFP - Ain1 FL
ABS2-1A
Δain1
pREP1
YFP - Ain1 FL
ABS3-2A
Δain1
pREP1 empty
leu1-32
pREP1 empty
-
-
-
++
++
YE + 1M KCl 18°C
YE 30°C

Fig. 4

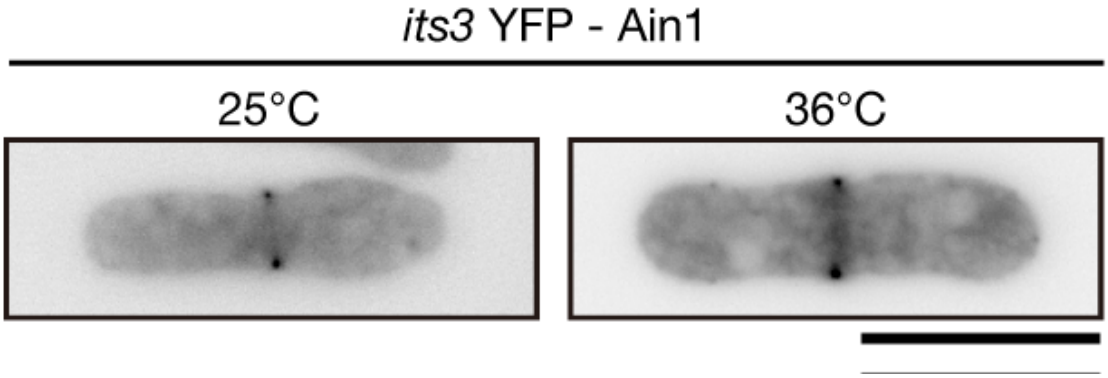

Fig. 5

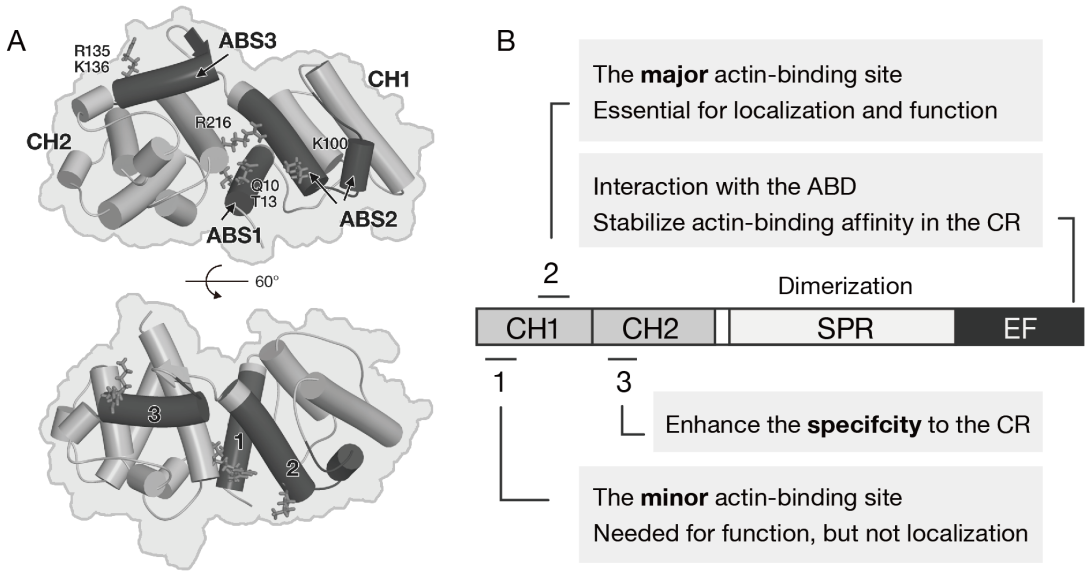
A
R135
K136
ABS3
CH1
CH2
R216
K100
Q10
T13
ABS1
ABS2
60°
3
1
2
B
The major actin-binding site
Essential for localization and function
Interaction with the ABD
Stabilize actin-binding affinity in the CR
2
Dimerization
CH1
CH2
SPR
EF
1
3
Enhance the specifcity to the CR
The minor actin-binding site
Needed for function, but not localization

Fig. 6

Supplemental Methods

Construction of strains

C-terminal GFP-tagged *ain1* strains (*ain1*$^{+}$*-gfp::kan*^{r} and *ain1ΔEF-gfp::kan*^{r}) were constructed by PCR-based homologous recombination (*1*). The following PCR primer pairs were used to amplify the F-fragments; 5'-GAAGCATTGCAAGGATGCAGGAGTACTGGC-3' (F1) and 5'-TTAATTAACCCGGGGATCCGAACTATTTCTTTGTCTTCGG-3' (R2) for *ain1*$^{+}$*-gfp::kan*^{r}, and F1 and 5'-TTAATTAACCCGGGGATCCGTTTAGTAATTCCGTCTAGTTC-3' (R3) for *ain1ΔEF-gfp::kan*^{r}. The R-fragment was amplified by 5'-GTTTAAACGAGCTCGAATTCAACGGAGCATTTTGAATCAC-3' (F2) and 5'-GTTATGCTATGCGAGCCATGTATATTCTTG-3' (R1). F- and R-fragments were both fused by PCR with *Sal*I-digested pFA6a-GFP(S65T)-KanMX6. *S. pombe* cells were transformed with amplified constructs using the lithium acetate method. YE medium containing 100 μg/mL G418 (Sigma-Aldrich) was used for the selection of drug-resistant transformants.

Western blot

Log-phase incubated cells were harvested and extracted by the NaOH treatment method (*2*, *3*). Protein extracts were subjected to 10% SDS-PAGE. Gels were transferred to PVDF membranes and probed with a mouse anti-GFP antibody (Roche). Horseradish peroxidase (HRP)-conjugated goat anti-mouse IgG (Santa Cruz Biotechnology) was used as a secondary antibody. Membranes were developed using ECL reagents (GE).

Supplemental data

Fig. S1 Artificially synthesized *ain1*$^+$ gene

The nucleotide sequence of the open reading frame of an artificially synthesized *ain1*$^+$ gene is shown. Several triplets are replaced with another synonymous codon for stronger expression according to the codon usage table of *S. pombe* (*4*) and *E. coli* (http://www.kazusa.or.jp/codon/cgi-bin/showcodon.cgi?species=83333).

Fig. S2 Control experiment of the low-speed co-sedimentation assay

Ain1FL (0.5–8 μM) alone was centrifuged at low-speed as in Fig. 2B. The supernatant (S) and pellet (P) were separated by SDS-PAGE and stained with CBB **(A)**. Amounts of Ain1 FL in the supernatant versus pellet were plotted **(B)**. About 16% of Ain1 FL was detected in the pellet fractions probably because of their adhesion to the internal walls of centrifuge tubes.

Fig. S3 Co-localization of an Ain1-mutated protein with actin

Cells expressing Lifeact-4×mCherry were transformed with vectors for the expression of the proteins indicated above and observed as in Figure 3A. Images of YFP-Ain1 (green) and Lifeact-4×mCherry (red) were merged. Asterisks indicate a mutation site. Arrows indicate the CR, and arrowheads indicate cortical dots.

Fig. S4 Overexpression of the CH1 of Ain1

Lifeact-4×mCherry-expressing cells that were transformed with pREP1YFP-ain1FL or -ain1CH1 were incubated at 30ºC for 18 h after removing thiamine from the cell culture to induce the overproduction of the protein. Cells treated with 1% DMSO with or without 8 μM Latrunculin-A (Lat-A) were observed. Note that abnormal cables decorated with Ain1 CH1 and Lifeact-4×mCherry remained, even in the presence of Lat-A. The bar shows 10 μm.

Fig. S5 Expression of fluorescent protein-tagged Ain1ΔEF

(A, C) Western blot of N-terminal YFP- or C-terminal GFP-tagged-Ain1. Arrowheads indicate tagged Ain1FL (98 kDa) and tagged Ain1ΔEF (83 kDa). **(B)** Localization of Ain1FL-GFP or Ain1ΔEF-GFP in mitotic cells. The bar shows 10 μm.

Table S1. Plasmids used in this study

plasmid	gene product (a. a.)	comment
pREP1		empty vector
pREP1YFP-ain1FL	1–621	Full-length protein
pREP1YFP-ain1ABD	1–235	actin-binding domain only
pREP1YFP-ain1CH1	1–122	CH1 domain only
pREP1YFP-ain1CH2	123–235	CH2 domain with an extra 5 residues GGRSR in the N terminus
pREP1YFP-ain1ΔCH1	123–621	Ain1ΔCH1 with GGRSR in the N terminus
pREP1YFP-ain1FL R216E	1–621, R216E	Arg216 was replaced with Glu
pREP1YFP-ain1ABD R216E	1–235, R216E	actin-binding domain only Arg216 was replaced with Glu
pREP1YFP-ain1ΔEF	1–490	C-terminal region containing the EF-hand was removed
pREP1YFP-ain1EF	491–621	C-terminal region containing the EF-hand with GGRSR in the N terminus
pREP1YFP-ain1ΔABD	236–621	Ain1ΔABD with GGRSR in the N terminus
pREP1YFP-ain1ΔEF R216E	1–490, R216E	The EF-hand was removed Arg216 was replaced with Glu
pREP1YFP-ain1FL ABS1-2A	1–621, Q10A, T13A	Q10 and T13 were replaced with Ala
pREP1YFP-ain1CH1 ABS1-2A	1–122, Q10A, T13A	CH1 domain only Q10 and T13 were replaced with Ala
pREP1YFP-ain1FL R216E ABS1-2A	1–621, R216E, Q10A, T13A	Q10 and T13 were replaced with Ala Arg216 was replaced with Glu
pREP1YFP-ain1FL ABS2-1A	1–621, K100A	K100 was replaced with Ala
pREP1YFP-ain1CH1 ABS2-1A	1–122, K100A	CH1 domain only K100 was replaced with Ala
pREP1YFP-ain1FL R216E ABS2-1A	1–621, R216E, K100A	K100 was replaced with Ala Arg216 was replaced with Glu
pREP1YFP-ain1FL ABS3-2A	1–621, R135A, K136A	R135, and K136 were replaced with Ala
pREP1YFP-ain1ΔCH1 ABS3-2A	123–621, R135A, K136A	Ain1ΔCH1 with GGRSR in the N terminus R135 and K136 were replaced with Ala

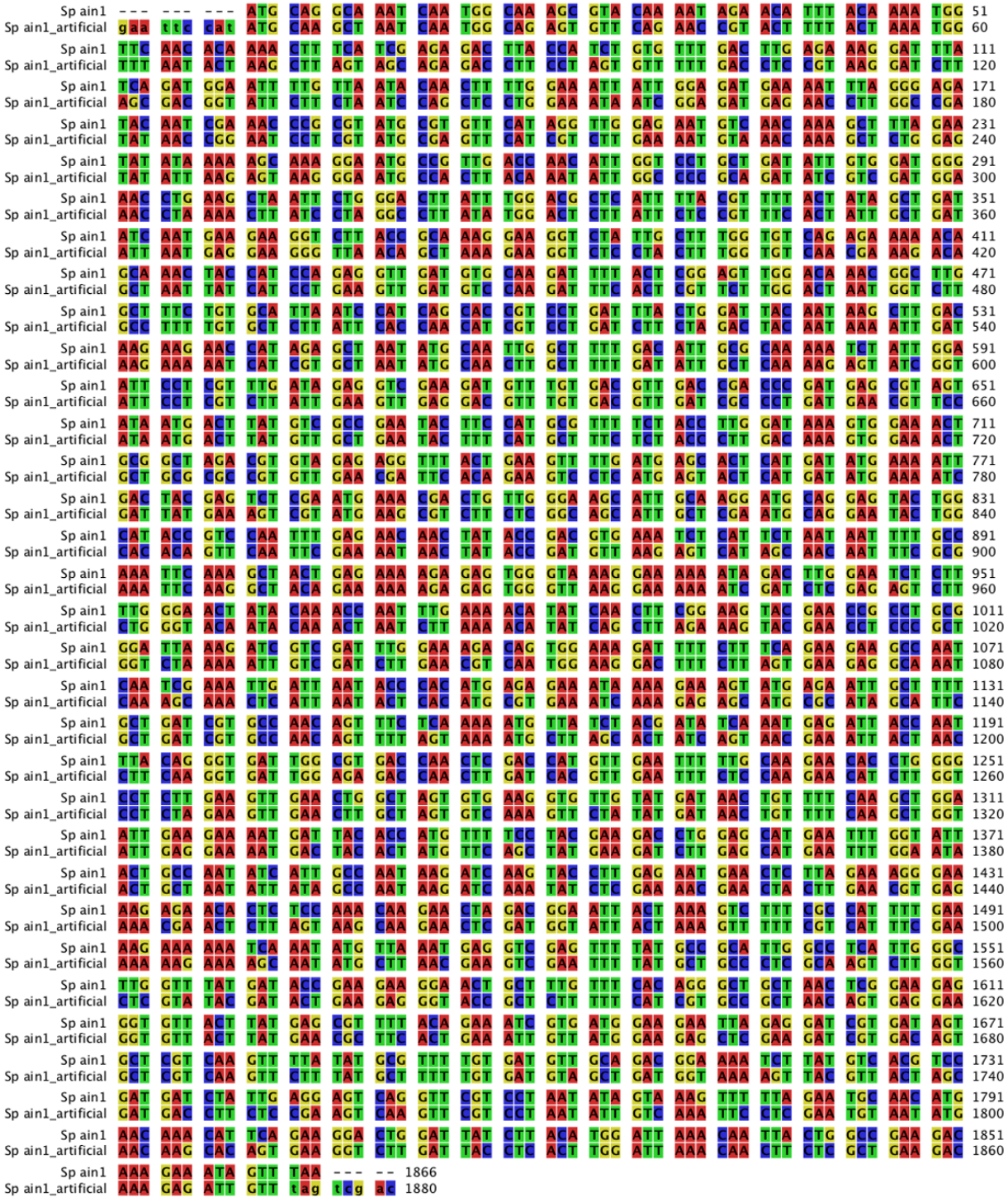
Sp ain1 --- --- --- ATG CAG GCA AAT CAA TGG CAA AGC GTA CAA AAT AGA ACA TTT ACA AAA TGG 51
Sp ain1_artificial gaa ttc cat ATG CAA GCT AAT CAA TGG CAG AGT GTT CAG AAC CGT ACT TTT ACT AAA TGG 60
Sp ain1 TTC AAC ACA AAA CTT TCA TCG AGA GAC TTA CCA TCT GTG TTT GAC TTG AGA AAG GAT TTA 111
Sp ain1_artificial TTT AAT ACT AAG CTT AGT AGC AGA GAC CTT CCT AGT GTT TTT GAC CTC CGT AAG GAT CTT 120
Sp ain1 TCA GAT GGA ATT TTG TTA ATA CAA CTT TTG GAA ATT ATT GGA GAT GAA AAT TTA GGG AGA 171
Sp ain1_artificial AGC GAC GGT ATT CTT CTA ATC CAG CTC CTG GAA ATA ATC GGA GAT GAG AAC CTT GGC CGA 180
Sp ain1 TAC AAT CGA AAC CCG CGT ATG CGT GTT CAT AGG TTG GAG AAT GTC AAC AAA GCT TTA GAA 231
Sp ain1_artificial TAT AAC CGG AAT CCT CGT ATG CGA GTT CAT CGT CTT GAA AAT GTA AAC AAA GCT CTG GAG 240
Sp ain1 TAT ATA AAA AGC AAA GGA ATG CCG TTG ACC AAC ATT GGT CCT GCT GAT ATT GTG GAT GGG 291
Sp ain1_artificial TAT ATT AAG AGT AAG GGA ATG CCA CTT ACA AAT ATT GGC CCC GCA GAT ATC GTC GAT GGA 300
Sp ain1 AAC CTG AAG CTA ATT CTG GGA CTT ATT TGG ACG CTC ATT TTA CGT TTT ACT ATA GCT GAT 351
Sp ain1_artificial AAC CTA AAA CTT ATC CTA GGC CTT ATA TGG ACT CTT ATT CTC CGT TTC ACT ATT GCT GAT 360
Sp ain1 ATC AAT GAA GAA GGT CTT ACC GCA AAG GAA GGT CTA TTG CTT TGG TGT CAG AGA AAA ACA 411
Sp ain1_artificial ATT AAT GAG GAA GGG TTA ACA GCT AAA GAA GGT CTC CTA CTT TGG TGT CAA CGA AAG ACA 420
Sp ain1 GCA AAC TAC CAT CCA GAG GTT GAT GTG CAA GAT TTT ACT CGG AGT TGG ACA AAC GGC TTG 471
Sp ain1_artificial GCT AAT TAT CAT CCT GAA GTT GAT GTC CAA GAT TTC ACT CGT TCT TGG ACT AAT GGT CTT 480
Sp ain1 GCT TTC TGT GCA TTA ATC CAT CAG CAC CGT CCT GAT TTA CTG GAT TAC AAT AAG CTT GAC 531
Sp ain1_artificial GCC TTT TGT GCT CTT ATT CAC CAA CAT CGT CCT GAT CTT CTA GAC TAC AAT AAA ATT GAT 540
Sp ain1 AAG AAG AAC CAT AGA GCT AAT ATG CAA TTG GCT TTT GAC ATT GCG CAA AAA TCT ATT GGA 591
Sp ain1_artificial AAG AAA AAT CAT CGT GCT AAT ATG CAA CTT GCT TTT GAT ATT GCT CAA AAG AGT ATC GGT 600
Sp ain1 ATT CCT CGT TTG ATA GAG GTC GAA GAT GTT TGT GAC GTT GAC CGA CCC GAT GAG CGT AGT 651
Sp ain1_artificial ATT CCT CGT CTT ATT GAA GTT GAG GAC GTT TGT GAC GTT GAT CGC CCT GAT GAA CGT TCC 660
Sp ain1 ATA ATG ACT TAT GTC GCC GAA TAC TTC CAT GCG TTT TCT ACC TTG GAT AAA GTG GAA ACT 711
Sp ain1_artificial ATA ATG ACT TAT GTT GCT GAA TAC TTT CAT GCT TTC TCT ACC CTT GAC AAA GTG GAA ACT 720
Sp ain1 GCG GCT AGA CGT GTA GAG AGG TTT ACT GAA GTT TTG ATG AGC ACT CAT GAT ATG AAA ATT 771
Sp ain1_artificial GCT GCG CGC CGT GTT GAA CGA TTC ACA GAA GTC CTC ATG AGT ACT CAT GAT ATG AAA ATC 780
Sp ain1 GAC TAC GAG TCT CGA ATG AAA CGA CTG TTG GGA AGC ATT GCA AGG ATG CAG GAG TAC TGG 831
Sp ain1_artificial GAT TAT GAA AGT CGT ATG AAG CGT CTT CTC GGC AGC ATT GCT CGA ATG CAG GAA TAC TGG 840
Sp ain1 CAT ACC GTC CAA TTT GAG AAC AAC TAT ACC GAC GTG AAA TCT CAT TCT AAT AAT TTT GCC 891
Sp ain1_artificial CAC ACA GTT CAA TTC GAA AAT AAC TAT ACC GAT GTT AAG AGT CAT AGC AAC AAT TTC GCG 900
Sp ain1 AAA TTC AAA GCT ACT GAG AAA AGA GAG TGG GTA AAG GAA AAA ATA GAC TTG GAA TCT CTT 951
Sp ain1_artificial AAA TTC AAG GCT ACA GAA AAA AGA GAG TGG GTT AAG GAA AAA ATC GAT CTC GAG AGT CTT 960
Sp ain1 TTG GGA ACT ATA CAA ACC AAT TTG AAA ACA TAT CAA CTT CGG AAG TAC GAA CCG CCT GCG 1011
Sp ain1_artificial CTG GGT ACA ATA CAA ACT AAT CTT AAA ACA TAT CAG CTT AGA AAG TAC GAA CCT CCC GCT 1020
Sp ain1 GGA TTA AAG ATC GTC GAT TTG GAA AGA CAG TGG AAA GAT TTT CTT TCA GAA GAA GCC AAT 1071
Sp ain1_artificial GGT CTA AAA ATT GTC GAT CTT GAA CGT CAA TGG AAG GAC TTT CTT AGT GAA GAG GCA AAT 1080
Sp ain1 CAA TCG AAA TTG ATT AAT ACC CAC ATG AGA GAA ATA AAA GAA AGT ATG AGA ATT GCT TTT 1131
Sp ain1_artificial CAA AGC AAA CTC ATT AAT ACT CAC ATG CGT GAA ATC AAA GAG AGC ATG CGC ATA GCA TTC 1140
Sp ain1 GCT GAT CGT GCC AAC AGT TTC TCA AAA ATG TTA TCT ACG ATA TCA AAT GAG ATT ACC AAT 1191
Sp ain1_artificial GCT GAT CGT GCC AAC AGT TTT AGT AAA ATG CTT AGC ACT ATC AGT AAC GAA ATT ACT AAC 1200
Sp ain1 TTA CAG GGT GAT TGG CGT GAC CAA CTC GAC CAT GTT GAA TTT TTG CAA GAA CAC CTG GGG 1251
Sp ain1_artificial CTT CAA GGT GAT TGG AGA GAC CAA CTT GAT CAC GTT GAA TTT CTC CAA GAA CAT CTT GGT 1260
Sp ain1 CCT CTT GAA GTT GAA CTG GCT AGT GTG AAG GTG TTG TAT GAT AAC TGT TTT CAA GCT GGA 1311
Sp ain1_artificial CCT CTA GAA GTT GAA CTT GCT AGT GTC AAA GTT CTA TAT GAT AAC TGT TTT CAA GCT GGT 1320
Sp ain1 ATT GAA GAA AAT GAT TAC ACC ATG TTT TCC TAC GAA GAC CTG GAG CAT GAA TTT GGT ATT 1371
Sp ain1_artificial ATT GAG GAA AAT GAC TAC ACT ATG TTC AGC TAT GAA GAT CTT GAG CAT GAA TTT GGA ATA 1380
Sp ain1 ACT GCC AAT ATC ATT GCC AAT AAG ATC AAG TAC CTT GAG AAT GAA CTC TTA GAA AGG GAA 1431
Sp ain1_artificial ACT GCT AAT ATT ATA GCC AAT AAG ATC AAA TAT CTC GAA AAC GAA CTA CTT GAA CGT GAG 1440
Sp ain1 AAG AGA ACA CTC TCC AAA CAA GAA CTA GAC GGA ATT ACT AAA GTC TTT CGC CAT TTT GAA 1491
Sp ain1_artificial AAA CGA ACT CTT AGT AAG CAA GAA CTC GAT GGT ATT ACT AAA GTT TTT CGT CAT TTC GAA 1500
Sp ain1 AAG AAA AAA TCA AAT ATG TTA AAT GAG GTC GAG TTT TAT GCC GCA TTG GCC TCA TTG GGC 1551
Sp ain1_artificial AAA AAG AAA AGC AAT ATG CTT AAC GAA GTC GAA TTT TAT GCT GCC CTC GCA AGT CTT GGT 1560
Sp ain1 TTG GTT TAT GAT ACC GAA GAA GGA ACT GCT TTG TTT CAC AGG GCT GCT AAC TCG GAA GAG 1611
Sp ain1_artificial CTC GTA TAC GAT ACT GAA GAG GGT ACC GCT CTT TTT CAT CGT GCC GCT AAC AGT GAG GAA 1620
Sp ain1 GGT GTT ACT TAT GAG CGT TTT ACA GAA ATC GTG ATG GAA GAA TTA GAG GAT CGT GAT AGT 1671
Sp ain1_artificial GGT GTT ACT TAT GAA CGC TTC ACT GAA ATT GTT ATG GAA GAG CTC GAA GAT CGT GAC AGT 1680
Sp ain1 GCT CGT CAA GTT TTA TAT GCG TTT TGT GAT GTT GCA GAC GGA AAA TCT TAT GTC ACG TCC 1731
Sp ain1_artificial GCT CGT CAA GTT CTT TAT GCT TTT TGT GAT GTA GCT GAT GGT AAA AGT TAC GTT ACT AGC 1740
Sp ain1 GAT GAT CTA TTG AGG AGT CAG GTT CGT CCT AAT ATA GTA AAG TTT TTA GAA TGC AAC ATG 1791
Sp ain1_artificial GAT GAC CTT CTC CGA AGT CAA GTT CGT CCT AAT ATT GTC AAA TTC CTC GAA TGT AAT ATG 1800
Sp ain1 AAC AAA CAT TCA GAA GGA CTG GAT TAT CTT ACA TGG ATT AAA CAA TTA CTG GCC GAA GAC 1851
Sp ain1_artificial AAC AAG CAC AGT GAA GGT CTT GAT TAC CTC ACT TGG ATT AAA CAA CTT CTC GCT GAA GAC 1860
Sp ain1 AAA GAA ATA GTT TAA --- -- 1866
Sp ain1_artificial AAA GAG ATT GTT tag tcg ac 1880

Fig. S1

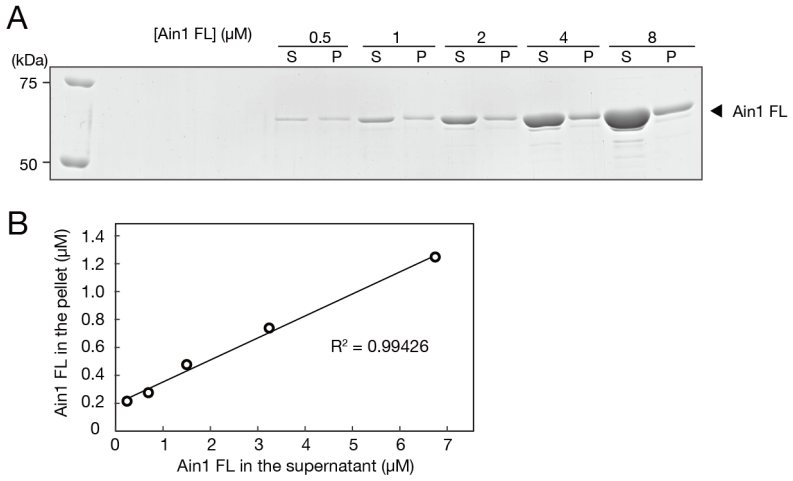
A
[Ain1 FL] (μM)
0.5
1
2
4
8
S P S P S P S P S P
(kDa)
75
50
Ain1 FL
B
Ain1 FL in the pellet (μM)
1.4
1.2
1.0
0.8
0.6
0.4
0.2
0
R² = 0.99426
0 1 2 3 4 5 6 7
Ain1 FL in the supernatant (μM)

Fig. S2

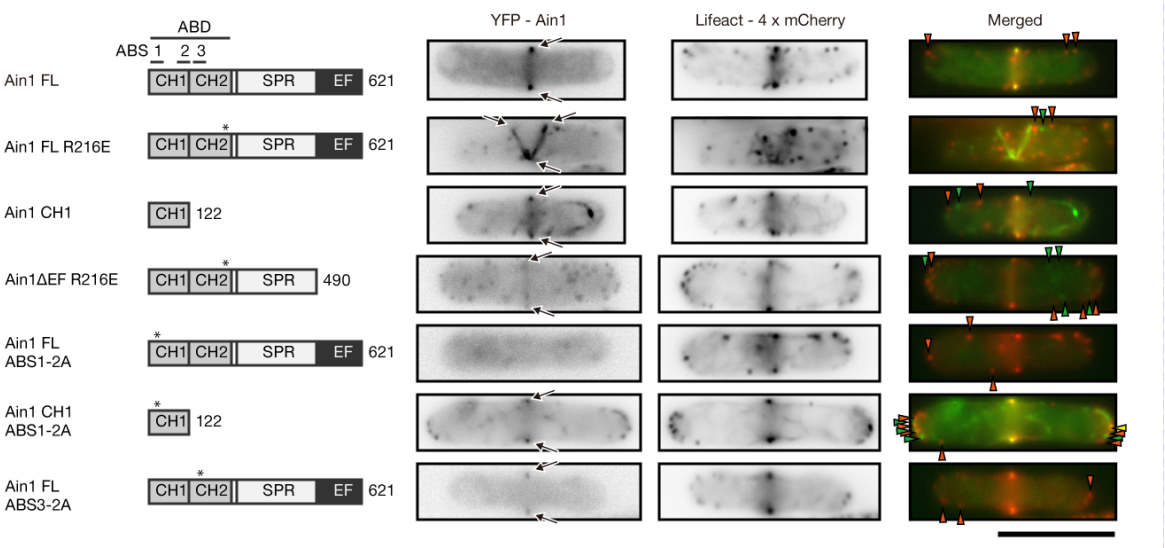
ABD
ABS 1 2 3
Ain1 FL
CH1 CH2 SPR EF 621
Ain1 FL R216E
CH1 CH2 SPR EF 621
Ain1 CH1
CH1 122
Ain1ΔEF R216E
CH1 CH2 SPR 490
Ain1 FL
ABS1-2A
CH1 CH2 SPR EF 621
Ain1 CH1
ABS1-2A
CH1 122
Ain1 FL
ABS3-2A
CH1 CH2 SPR EF 621
YFP - Ain1
Lifeact - 4 x mCherry
Merged

Fig. S3

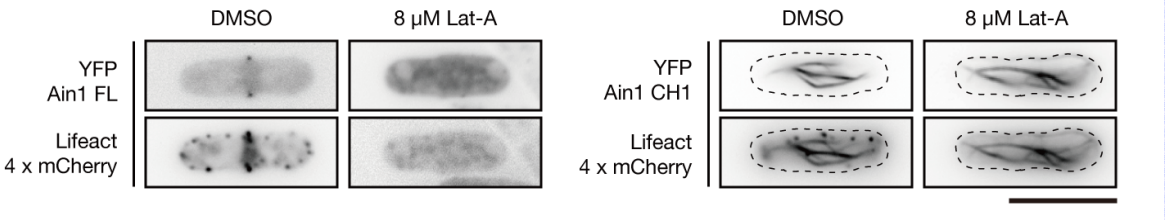
DMSO
8 µM Lat-A
YFP
Ain1 FL
Lifeact
4 x mCherry
DMSO
8 µM Lat-A
YFP
Ain1 CH1
Lifeact
4 x mCherry

Fig. S4

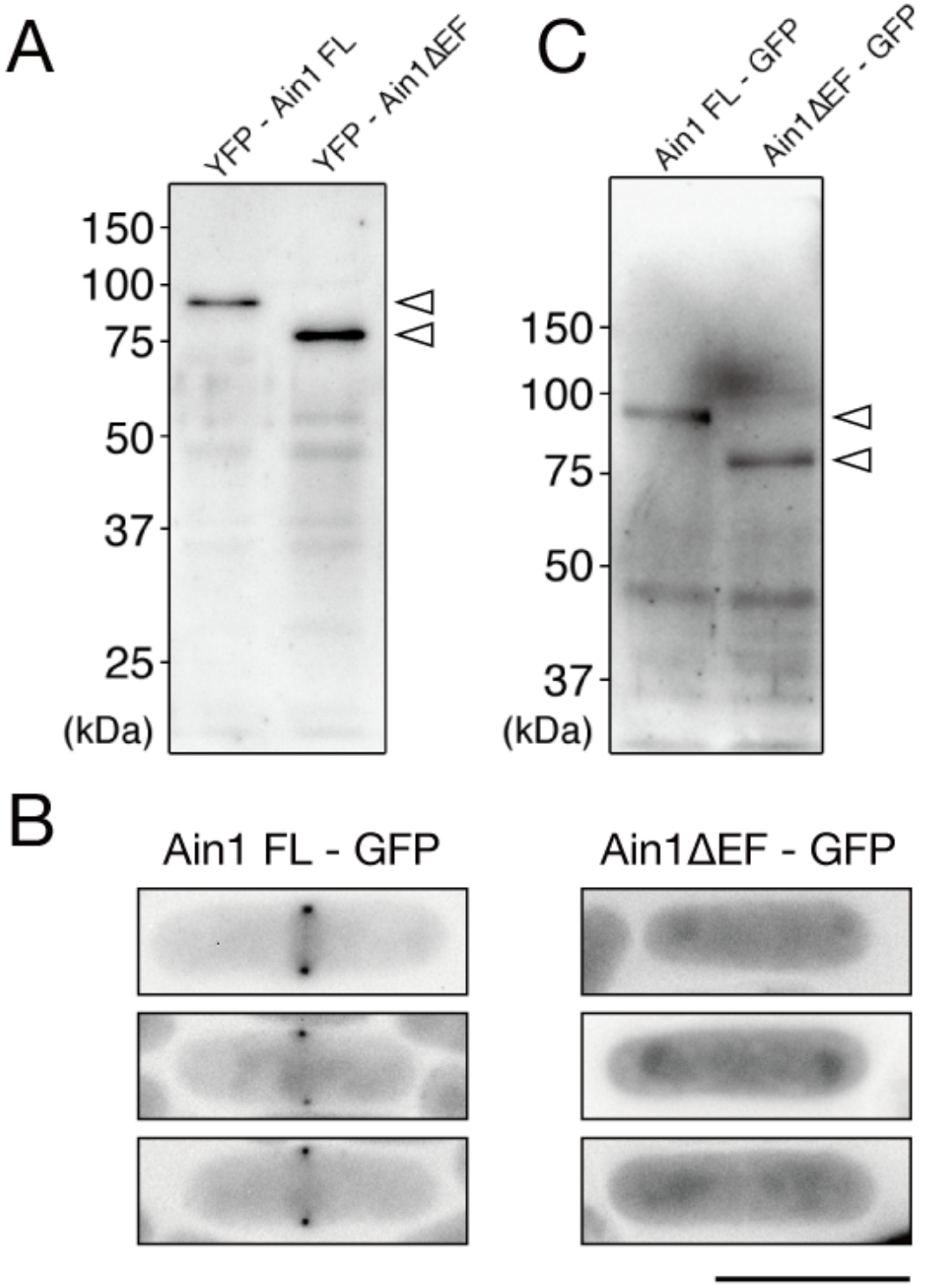
A
YFP - Ain1 FL
YFP - Ain1ΔEF
150
100
75
50
37
25
(kDa)
C
Ain1 FL - GFP
Ain1ΔEF - GFP
150
100
75
50
37
(kDa)
B
Ain1 FL - GFP
Ain1ΔEF - GFP

Fig. S5